

Inertial stochastic dynamics. II. Influence of inertia on slow kinetic processes of supercoiled DNA

Daniel A. Beard and Tamar Schlick^{a)}

*Department of Chemistry and Courant Institute of Mathematical Sciences, New York University
and Howard Hughes Medical Institute, 251 Mercer Street, New York, New York 10012*

(Received 13 October 1999; accepted 8 February 2000)

We apply our new algorithms presented in the companion paper (LTID: long-time-step inertial dynamics, IBD: inertial Brownian dynamics) for mass-dependent Langevin dynamics (LD) with hydrodynamics, as well as the standard Brownian dynamical (BD) propagator, to study the thermal fluctuations of supercoiled DNA minicircles. Our DNA model accounts for twisting, bending, and salt-screened electrostatic interactions. Though inertial relaxation times are on the order of picoseconds, much slower kinetic processes are affected by the Brownian (noninertial) approximation typically employed. By comparing results of LTID and IBD to those generated using the standard (BD) algorithm, we find that the equilibrium fluctuations in writhing number, Wr , and radius of gyration, R_g , are influenced by mass-dependent terms. The autocorrelation functions for these quantities differ between the BD simulations and the inertial LD simulations by as much as 10%. In contrast, when the nonequilibrium process of relaxation from a perturbed state is examined, all methods (inertial and diffusive) yield similar results with no detectable statistical differences between the mean folding pathways. Thus, while the evolution of an ensemble toward equilibrium is equally well described by the inertial and the noninertial methods, thermal fluctuations are influenced by inertia. Examination of such equilibrium fluctuations in a biologically relevant macroscopic property—namely the two-site intermolecular distance—reveals mass-dependent behavior: The rate of juxtaposition of linearly distant sites along a 1500-base pair DNA plasmid, occurring over time scales of milliseconds and longer, is increased by about 8% when results from IBD are compared to those from BD. Since inertial modes that decay on the picosecond time scale in the absence of thermal forces exert an influence on slower fluctuations in macroscopic properties, we advocate that IBD be used for generating long-time trajectories of supercoiled DNA systems. IBD is a practical alternative since it requires modest computational overhead with respect to the standard BD method. © 2000 American Institute of Physics. [S0021-9606(00)50817-4]

I. INTRODUCTION

In the previous article¹ we introduced two new algorithms for integrating the inertial Langevin equation with hydrodynamic coupling between the particles in a system: LTID (long-time-step inertial dynamics) and IBD (inertial Brownian dynamics). In Ref. 1, we showed that LTID, while employing time steps longer than the inertial relaxation times, is a consistent numerical integrator for the Langevin equation and captures inertial effects ignored by Brownian dynamics (BD). IBD is a cheaper inertial integrator which is more accurate than BD (in terms of the statistical properties of Langevin trajectories) for time steps comparable to those used in BD. Here we compare the dynamics of elastic models of supercoiled DNA systems based on the two inertial algorithms to that based on the noninertial (BD) algorithm of Ermak and McCammon.²

We show that all three simulation algorithms appropriately sample the configurational space of the canonical ensemble by comparing the realized probability distributions of two global DNA descriptors—writhing number, Wr , and ra-

dius of gyration, R_g —to those generated by Monte Carlo sampling for a 600-base pair (bp) DNA plasmid. In addition, estimates of the translational diffusion coefficient, a measure sensitive to the distribution of molecular configurations, agree for the three schemes. This agreement, used to validate IBD and LTID, is expected as neither equilibrium configuration distributions nor molecular diffusion coefficients depend on the mass of the particles in the system. However, mass may influence the rate of transition between configurations.

Indeed, for our DNA model, we find that certain dynamic properties (e.g., autocorrelation functions of the geometric descriptors Wr and R_g) are sensitive to the diffusive approximation made in BD. Although inertial relaxation-time constants are on the order of picoseconds, there exists a non-negligible coupling between fast (picosecond) and slow (microsecond) processes. This coupling influences the kinetics of global conformational changes in a mass-dependent manner. Using the autocorrelation function as a convenient measure of the rate of fluctuation of stationary stochastic variables, we note differences between the massless and the inertial systems of 1% and 10% for the rates of Wr and R_g fluctuation, respectively.

^{a)}Author to whom correspondence should be addressed; electronic mail: schlick@nyu.edu

The behavior predicted in the low-time-step limit of LTID is an accurate representation of inertial dynamics as governed by the Langevin equation. This was shown in Ref. 1 by comparing computational to theoretical results. LTID is semianalytical, based on propagating the frictional modes over finite time steps, and is thus more expensive than IBD and BD. However, the LTID autocorrelation functions provide a benchmark of correlation structure to which the results from IBD and BD can be compared. We show that IBD, based on a singular perturbative expansion of the Langevin equation, matches the inertial behavior of the Langevin equation when the numerical time step is chosen appropriately. Since IBD is much less computationally expensive than LTID and is competitive with BD in terms of CPU usage, we show that the IBD algorithm can be used (at a relatively modest computational cost over BD protocols) when inertial effects may be important.

We demonstrate this by using IBD to simulate the inertial dynamics of systems on size and time scales previously accessible only to BD. Specifically, we analyze the effects of inertia on the biologically important process of site *juxtaposition*. This process refers to the close spatial approach of linearly distant sites along the DNA contour. DNA site juxtaposition can depend critically on superhelicity^{3–5} and is important for site-specific recombination reactions^{6,7} in prokaryotes. Juxtaposition also plays a role in other processes, such as transcription initiation, where distant DNA domains interact, often through protein modulation. The influence of supercoiling on the dynamics of juxtaposition has already been studied using BD simulations of DNA plasmids ranging in size from 600 to 3000 bp.⁸ Calculations have focused on estimating juxtaposition times as a function of DNA superhelicity, site separation,⁸ and the ionic environment, as well as on deducing the responsible mechanisms.⁹ We show here that the mean juxtaposition times for 1200- and 1500-bp plasmids depend on whether an inertial or non-inertial algorithm is used. The rate of fluctuations in intermolecular distance increases and the mean juxtaposition time decreases by 6% and 8% when inertia is incorporated in 1200-bp and 1500-bp systems, respectively. An 8% difference in mean juxtaposition time for the 1500-bp system corresponds to a difference of about 30 μ s between the IBD and BD formulations. This difference is surprisingly large on the picosecond time scale of the frictional relaxation of the inertial modes.

As another application of inertial dynamics, we studied the relaxation from a torsionally stressed planar circle to a supercoiled state. From a large ensemble of folding trajectories (~ 500) computed using LTID, IBD, and BD, we do not detect any statistically significant differences between the predictions of the three algorithms.

These examples show that mean folding pathways to equilibrium are weakly mass dependent, while slow kinetic processes resulting from equilibrium fluctuations are sensitive to inertia. For the biologically important juxtaposition process, our algorithm IBD is a preferred scheme.

In Sec. II we present the computational model for the DNA structure and energetics and the detailed implementa-

tion of LTID, IBD, and BD for the DNA model. In Sec. III, we present the following results:

- (1) CPU—analysis of the computational costs associated with the two new algorithms in comparison to the performance of BD,
- (2) internal time scales—computed frictional eigenmodes for equilibrium configurations used to calculate the time scale for the slithering motion of a 1500-bp system,
- (3) equilibrium motions—translational diffusion coefficients, equilibrium configuration distributions for W_r and R_g , and the W_r and R_g autocorrelation functions for a 600-bp supercoil calculated from LTID, IBD, and BD trajectories,
- (4) juxtaposition kinetics—mean juxtaposition times from equilibrium trajectories of 600-, 900-, 1200-, and 1500-bp supercoils based on IBD and BD,
- (5) nonequilibrium motions—ensemble folding from a perturbed state to equilibrium of a 600-bp system, calculated using LTID, IBD, and BD.

We conclude in Sec. IV by summarizing inertia's significant influence on the time scales of thermal motions contrasted to its lack of influence on the mean motion of a statistical ensemble, and by recommending IBD as a viable alternative to the standard BD scheme.

II. METHODS

We have developed feasible methods for simulating the dynamic behavior of macroscopic models of biopolymer systems governed by the inertial LD equation with hydrodynamic interactions.¹ Here, we apply these methods to a computational model of supercoiled DNA.

A. The DNA model

The bead model of supercoiled DNA that we use here has been introduced and characterized by our group^{10,8} and by others.^{11–15} Appropriate parameter values reproduce experimentally observed properties of large DNA. Though prior studies of the dynamics of this model have used BD, the values for the model parameters (such as bending and twisting elasticity constants) are expected to be equally valid for both the noninertial Brownian and the inertial Langevin descriptions of the dynamics since they are calibrated to reproduce properties, such as equilibrium configuration distributions and diffusion coefficients, that do not depend on the masses of the particles in the system.

The DNA system is represented by a series of N connected beads. A closed DNA loop is modeled by connecting bead $i=N$ to bead $i=1$. Associated with each bead i is a position, r_i , and a local coordinate system of vectors $\{a_i, b_i, c_i\}$ which define the rotational orientation of the chain. A complete description of a conformation of the system requires specification of both the position vector r and the $\{a, b, c\}$ triplet for $i=1, \dots, N$. Alternatively, one can specify the position vector and the Euler angles $\{\alpha_i, \beta_i, \gamma_i\}$, to describe the rotation of the $(i-1)$ th to the i th coordinate system for each successive bead.¹¹

The potential energy is modeled as the sum of four terms:

$$E = E_s + E_b + E_t + E_e, \quad (1)$$

to account for stretching, bending, twisting, and electrostatic interactions, as follows.

The stretching energy, E_s , is computed from

$$E_s = \frac{h}{2} \sum_{i=1}^N (\|r_i - r_{i+1}\| - l_0)^2, \quad (2)$$

where l_0 is the resting length of each interbead segment and $l_0 = L/N$ (4 nm here), where L is the target length of the DNA molecule. The stretching energy is considered a computational device to restrain the length of the DNA to the target length. Setting the stretching constant to $h = 1500; k_B T / l_0^2$ results in deviations in realized segment lengths of less than 1% of l_0 .

The bending energy, E_b , is calculated from the set of angles $\{\beta_i\}$, denoting the deformation between the $(i-1)$ th and the i th segments:

$$E_b = \frac{A}{2l_0} \sum_{i=1}^N \beta_i^2, \quad (3)$$

where A denotes the bending rigidity constant, which is expressed as $A = L_p k_B T$, corresponding to $A/l_0 = 12.5 k_B T$ for a bending persistence length $L_p = 50$ nm,¹⁶ and a segment length of $l_0 = 4$ nm.

The torsional angle between beads $(i-1)$ and i is given by the sum of the Euler angles $\alpha_i + \gamma_i$, and the torsional energy, E_t , is calculated as

$$E_t = \frac{C}{2l_0} \sum_{i=1}^N (\alpha_i + \gamma_i - \phi_0)^2, \quad (4)$$

where ϕ_0 is the equilibrium excess twist due to superhelical winding:

$$\phi_0 = 2\pi\sigma(l_0/l_h). \quad (5)$$

Here σ is the superhelical density, and l_h is the DNA helical repeat length of about 3.55 nm. The torsional rigidity constant is set to $C = 3 \times 10^{-12}$ erg nm.¹⁵

The electrostatic energy is approximated by the Debye–Hückel potential associated with point charges located at the centers of the beads:

$$E_e = \frac{(\nu l_0)^2}{\epsilon} \sum_{j>i+1} \frac{e^{-\kappa r_{ij}}}{r_{ij}}, \quad (6)$$

where ν is the effective linear charge density along the chain, ϵ is the dielectric constant of water, $1/\kappa$ is the Debye length, and r_{ij} is the scalar distance between beads i and j . The value of ν is parametrized according to the method of Stigter¹⁷ so that the far-field potential predicted by Eq. (6) matches the solution to the nonlinear Poisson–Boltzmann equation for a charged cylinder in an ionic solvent. For a monovalent salt concentration of 0.04 M, $1/\kappa = 1.52$ nm and $\nu = -3.92$ e nm⁻¹.

We use the radius of gyration (R_g) and the writhing number (Wr) as convenient measures of the macroscopic structure of our supercoiled DNA model. The writhing num-

ber describes the number of self-crossings of the closed DNA helical axis, averaged over all planar projections of the three-dimensional space curve (thus it is generally nonintegral). It can be approximated using the following discretization of the Gauss double integral:¹²

$$Wr = \frac{1}{4\pi} \sum_{j=1}^N \sum_{i \neq j} \frac{(r_{j+1} - r_j) \times (r_{j+i} - r_i) \cdot (r_j - r_i)}{\|r_j - r_i\|^3}. \quad (7)$$

The radius of gyration is a measure of the DNA polymer size. It is defined as the root-mean-square displacement of the hydrodynamic bead centers from the center of mass:¹⁸

$$R_g^2 = \frac{1}{N} \sum_{i=1}^N \left\| r_i - \frac{1}{N} \sum_{i=1}^N r_i \right\|^2. \quad (8)$$

B. Hydrodynamics calculations

The movements of the components of the DNA model are coupled to one another through the action of the viscous medium. This viscous coupling is approximated by incorporating either the configuration-dependent friction tensor \mathbf{Z} into the LD equation, or the diffusion tensor \mathbf{D} into the IBD and BD equations as previously outlined. For IBD and BD we use the Rotne–Prager diffusion tensor.¹⁹ For the LTID algorithm, we construct \mathbf{Z} from the inverse of the Rotne–Prager diffusion tensor.

For an N -bead system \mathbf{D} is a $3N \times 3N$ matrix written as

$$\mathbf{D} = \begin{bmatrix} \mathbf{D}_{11} & \mathbf{D}_{12} & \cdots & \mathbf{D}_{1N} \\ \mathbf{D}_{21} & \mathbf{D}_{22} & \cdots & \mathbf{D}_{2N} \\ \vdots & \vdots & \ddots & \vdots \\ \mathbf{D}_{N1} & \mathbf{D}_{N2} & \cdots & \mathbf{D}_{NN} \end{bmatrix}, \quad (9)$$

where each \mathbf{D}_{ij} is a 3×3 matrix representing the interaction between the i th and j th beads. For the Rotne–Prager tensor, each \mathbf{D}_{ij} is calculated from¹⁹

$$\mathbf{D}_{ij} = \begin{cases} \left(\frac{k_B T}{3\pi\eta d} \right) \mathbf{I} & \text{for } i=j \text{ (same bead)} \\ \left(\frac{k_B T}{8\pi\eta\|r_{ij}\|} \right) \left[\left(\mathbf{I} + \frac{r_{ij} r_{ij}^T}{r_{ij}^2} \right) + \frac{d^2}{2r_{ij}^2} \left(\frac{1}{3} \mathbf{I} - \frac{r_{ij} r_{ij}^T}{r_{ij}^2} \right) \right] & \text{for } i \neq j \text{ (different beads),} \end{cases} \quad (10)$$

where d is the bead diameter and η is the viscosity of the surrounding fluid. The vector r_{ij} is equal to $r_i - r_j$. The quantity r_{ij}^2 is equal to $\|r_i - r_j\|^2$.

C. Simulation algorithms

The simulation algorithms were introduced in Ref. 1. Here we present the implementation of LTID, IBD, and BD for the above-described DNA model. In the following sections, $v^n \in \mathfrak{R}^{3N}$ is the collective velocity vector for the n particles in the system at the n th time step. The vector $r^n \in \mathfrak{R}^{3N}$ is the collective position vector. The entries of the diagonal matrix $\mathbf{M} \in \mathfrak{R}^{3N \times 3N}$ are the masses of particles. The positive definite friction tensor $\mathbf{Z}(r(t)) \in \mathfrak{R}^{3N \times 3N}$ is related to the diffusion tensor by $\mathbf{Z} = k_B T \mathbf{D}^{-1}$.

1. LTID

The LTID algorithm requires an eigenmode decomposition of the matrix $\mathbf{A} = \mathbf{M}^{-1}\mathbf{Z} = k_B T \mathbf{M}^{-1} \mathbf{D}^{-1}$. In practice we construct the decomposition of \mathbf{A} by first factoring \mathbf{D} [which we have calculated from Eq. (10)]:

$$\mathbf{D} = \mathbf{L} \mathbf{\Sigma} \mathbf{L}^T, \quad (11)$$

where $\mathbf{\Sigma}$ is a diagonal matrix. Since our system is composed of beads of equal mass, m , the matrix \mathbf{A} can be written as

$$\mathbf{A} = \frac{k_B T}{m} (\mathbf{L} \mathbf{\Sigma} \mathbf{L}^T)^{-1} = \frac{k_B T}{m} \mathbf{L} \mathbf{\Sigma}^{-1} \mathbf{L}^T, \quad (12)$$

which is identical to the decomposition introduced in the companion paper,¹ $\mathbf{A} = \mathbf{L} \mathbf{\Lambda} \mathbf{L}^T$, where the entries of the diagonal matrix $\mathbf{\Lambda}$ are equal to $k_B T/m$ times the entries of the matrix $\mathbf{\Sigma}^{-1}$.

The correlation structure of the random force term can be expressed as

$$\langle f_r^m (f_r^n)^T \rangle = \frac{2k_B T \delta_{mn}}{\Delta t} \mathbf{Z} = \bar{\mathbf{L}} \bar{\mathbf{L}}^T \delta_{mn}, \quad (13)$$

where the subscripts n and m refer to time step, δ_{mn} is the usual Kronecker delta, and the matrix $\bar{\mathbf{L}}$ is a square root of the correlation matrix:

$$\bar{\mathbf{L}} = \sqrt{\left(\frac{2mk_B T}{\Delta t} \right)} \mathbf{L} \mathbf{\Lambda}^{1/2}. \quad (14)$$

According to the procedure outlined in Ref. 20, a random force vector having the proper correlation [Eq. (13)] can be calculated from the above via

$$f_r^n = \bar{\mathbf{L}} p, \quad (15)$$

where p is a vector of uncorrelated random numbers chosen from a Gaussian distribution with zero mean and unit variance. (See also Note added in proof in Ref. 1 of an alternative procedure.) Note that

$$\bar{\mathbf{L}} \bar{\mathbf{L}}^T = \frac{2mk_B T}{\Delta t} \mathbf{L} \mathbf{\Lambda} \mathbf{L}^T = \frac{2k_B T}{\Delta t} \mathbf{M} \mathbf{A} = \frac{2k_B T}{\Delta t} \mathbf{Z}.$$

For our DNA model, the torque on each bead acts only in the a_i direction and the random torque, τ_{r,a_i}^n , is chosen from a Gaussian distribution with zero mean and variance given by

$$\langle (\tau_{r,a_i}^n)^2 \rangle = \frac{2k_B T}{\Delta t} \xi_{a_i}. \quad (16)$$

LTID implementation for DNA model. Analogous to the application of LTID to a simple harmonic oscillator given in the companion paper,¹ we construct an algorithm that is second-order algorithm in its treatment of the systematic forces based on calculating a first-order estimate of the configuration at the $(n+1)$ th time step and using this configuration to make an estimate of the force acting at time $(n+1)$. We denote the first-order estimate of the configuration by the bead positions, $r^{n+1,*}$, and the local coordinate systems $\{a, b, c\}^{n+1,*}$.

For each bead, we first calculate an estimate of the finite rotation about the a_i axis:

$$\begin{aligned} \Delta \Theta_{a_i}^{n,*} &= \frac{m_{a_i}}{\xi_{a_i}} [1 - e^{-(\xi_{a_i}/m_{a_i})\Delta t}] \Omega_{a_i}^n \\ &+ \frac{1}{\xi_{a_i}} \left[\Delta t - \frac{m_{a_i}}{\xi_{a_i}} (1 - e^{-(\xi_{a_i}/m_{a_i})\Delta t}) \right] \\ &\times (\tau_{s,a_i}^n + \tau_{r,a_i}^n). \end{aligned} \quad (17)$$

The local coordinate system is then rotated by $\Delta \Theta_{a_i}^{n,*}$:

$$\begin{aligned} \tilde{a}_i^{n+1,*} &= a_i^n, \\ \tilde{b}_i^{n+1,*} &= \cos(\Delta \Theta_{a_i}^{n,*}) b_i^n + \sin(\Delta \Theta_{a_i}^{n,*}) c_i^n, \\ \tilde{c}_i^{n+1,*} &= -\sin(\Delta \Theta_{a_i}^{n,*}) b_i^n + \cos(\Delta \Theta_{a_i}^{n,*}) c_i^n. \end{aligned} \quad (18)$$

The tilde notation denotes the initial estimates of the coordinate axes after the rotation step alone. A further modification (described in the following) of the local coordinate axes is associated with the translation step because of the constraint that the beads rotate only about the a_i axes.

The initial estimate of the position coordinates is given by

$$\begin{aligned} r^{n+1,*} &= r^n + \mathbf{L} [\mathbf{\Lambda}^{-1} (\mathbf{I} - e^{-\mathbf{\Lambda} \Delta t})] \mathbf{L}^T v^n \\ &+ \mathbf{L} \mathbf{\Lambda}^{-1} [\mathbf{I} \Delta t - \mathbf{\Lambda}^{-1} (\mathbf{I} - e^{-\mathbf{\Lambda} \Delta t})] \mathbf{L}^T (g_s^n + g_r^n), \end{aligned} \quad (19)$$

where

$$g_s^n = -\mathbf{M}^{-1} \nabla E(r^n) \quad (20)$$

is the systematic acceleration acting on the r^n configuration, and g_r^n is the random acceleration due to the force f_r^n .

To enforce the constraint that the beads are free to rotate only about the a_i axes, we recompute the local coordinate systems of the particles after the position vector, $r^{n+1,*}$ has been calculated. Namely, we update a_i so that it remains tangent to the DNA segment:

$$a_i^{n+1,*} = (r_{i+1}^{n+1,*} - r_i^{n+1,*}) / \|r_{i+1}^{n+1,*} - r_i^{n+1,*}\|. \quad (21)$$

We define $\delta a_i^{n+1,*} = \tilde{a}_i^{n+1,*} - a_i^{n+1,*}$. Since we require all rotations about a_i to vanish, the new displacements are calculated:¹⁰

$$\delta b_i^{n+1,*} = -(\delta a_i^{n+1,*} \cdot \tilde{b}_i^{n+1,*}) \tilde{a}_i^{n+1,*} \quad (22)$$

and then $b_i^{n+1,*} = \tilde{b}_i^{n+1,*} + \delta b_i^{n+1,*}$. Then $b_i^{n+1,*}$ is determined as the component of $\tilde{b}_i^{n+1,*}$ perpendicular to $a_i^{n+1,*}$:

$$b_i^{n+1,*} = \frac{\tilde{b}_i^{n+1,*} - (\tilde{b}_i^{n+1,*} \cdot a_i^{n+1,*}) a_i^{n+1,*}}{\| \tilde{b}_i^{n+1,*} - (\tilde{b}_i^{n+1,*} \cdot a_i^{n+1,*}) a_i^{n+1,*} \|}. \quad (23)$$

Finally, $c_i^{n+1,*}$ can be calculated from the cross product:

$$c_i^{n+1,*} = a_i^{n+1,*} \times b_i^{n+1,*}. \quad (24)$$

Then using the first-order coordinates, we calculate an estimate of the systematic acceleration, $g_s^{n+1,*}$, and torques, $\tau_s^{n+1,*}$, acting on the system at the $(n+1)$ th time step.

The final update of angular velocity and position is obtained by averaging the systematic torque over the interval:

$$\Omega_{a_i}^{n+1} = \Omega_{a_i}^n e^{-(\xi_{a_i}/m_{a_i})\Delta t} + \frac{1}{\xi_{a_i}} [1 - e^{-(\xi_{a_i}/m_{a_i})\Delta t}] \times [\frac{1}{2}(\tau_{s,a_i}^n + \tau_{s,a_i}^{n+1,*}) + \tau_{r,a_i}^n], \quad (25)$$

$$\Delta \Theta_{a_i}^n = \frac{m_{a_i}}{\xi_{a_i}} [1 - e^{-(\xi_{a_i}/m_{a_i})\Delta t}] \Omega_{a_i}^n + \frac{1}{\xi_{a_i}} \left[\Delta t - \frac{m_{a_i}}{\xi_{a_i}} (1 - e^{-(\xi_{a_i}/m_{a_i})\Delta t}) \right] \times [\frac{1}{2}(\tau_{s,a_i}^n + \tau_{s,a_i}^{n+1,*}) + \tau_{r,a_i}^n]. \quad (26)$$

$$\tilde{a}_i^{n+1} = a_i^n, \quad \tilde{b}_i^{n+1} = \cos(\Delta \Theta_{a_i}^n) b_i^n + \sin(\Delta \Theta_{a_i}^n) c_i^n, \quad (27)$$

$$\tilde{c}_i^{n+1} = -\sin(\Delta \Theta_{a_i}^n) b_i^n + \cos(\Delta \Theta_{a_i}^n) c_i^n.$$

We then make the update of velocity and position by approximating the systematic acceleration acting over the time interval to be the average of g_r^n and $g_r^{n+1,*}$:

$$v^{n+1} = \mathbf{L} e^{-\Lambda \Delta t} \mathbf{L}^T v^n + \mathbf{L} \Lambda^{-1} (\mathbf{I} - e^{-\Lambda \Delta t}) \times \mathbf{L}^T [\frac{1}{2}(g_s^n + g_s^{n+1,*}) + g_r^n], \quad (28)$$

$$r^{n+1} = r^n + \mathbf{L} [\Lambda^{-1} (\mathbf{I} - e^{-\Lambda \Delta t})] \mathbf{L}^T v^n + \mathbf{L} \Lambda^{-1} [\mathbf{I} \Delta t - \Lambda^{-1} (\mathbf{I} - e^{-\Lambda \Delta t})] \mathbf{L}^T [\frac{1}{2}(g_s^n + g_s^{n+1,*}) + g_r^n]. \quad (29)$$

Finally, the calculation of the local coordinate axes, $\{a_i^{n+1}, b_i^{n+1}, c_i^{n+1}\}$ proceeds according to Eqs. (21)–(24).

2. IBD

Both the IBD and the BD algorithms are expressed in terms of the diffusion matrix \mathbf{D} and do not require an eigenmode decomposition of \mathbf{D} . If we define the random displacement, R^n , to be the displacement associated with the random force applied at the n th time step, we can express the IBD algorithm as

$$\Delta \Theta_{a_i}^n = \frac{1}{\xi_{a_i}} \left[\tau_{s,a_i}^n \Delta t + \frac{m_{a_i}}{\xi_{a_i}} (\tau_{s,a_i}^{n-1} - \tau_{s,a_i}^n) \right] + \Delta \Theta_{r,a_i}^n + \frac{m_{a_i}}{\xi_{a_i}} (\Delta \Theta_{r,a_i}^{n-1} - \Delta \Theta_{r,a_i}^n) / \Delta t, \quad (30)$$

$$r^{n+1} = r^n + \frac{\mathbf{D}}{k_B T} \left[f_s^n \Delta t + \frac{m \mathbf{D}}{k_B T} (f_s^{n-1} - f_s^n) \right] + R^n + \frac{m \mathbf{D}}{k_B T} (R^{n-1} - R^n) / \Delta t,$$

where f_s^n is the system force acting at the n th time step. The random displacements are correlated according to

$$\langle (R^m) \cdot (R^n)^T \rangle = 2 \Delta t \delta_{mn} \mathbf{D}. \quad (31)$$

This is the familiar random displacement used in the standard BD algorithm. The random displacements can be calculated from:²

$$R^n = \bar{\mathbf{L}} p, \quad (32)$$

where $\bar{\mathbf{L}}$ comes from the Cholesky factorization, $2 \Delta t \mathbf{D} = \bar{\mathbf{L}} \bar{\mathbf{L}}^T$, and again, p is a vector of uncorrelated random numbers chosen from a Gaussian distribution with zero mean and unit variance. The random angular displacements are chosen from Gaussian distribution with variance given by

$$\langle (\Delta \Theta_{r,a_i}^n)^2 \rangle = \frac{2 k_B T \Delta t}{\xi_{a_i}}. \quad (33)$$

IBD implementation for DNA model. Analogous to the LTID implementation, a second-order estimate of the systematic force is used to update the position at each time step. An initial estimate of the position and rotations is made according to

$$\Delta \Theta_{a_i}^{n,*} = \frac{1}{\xi_{a_i}} \left[\tau_{s,a_i}^n \Delta t + \frac{m_{a_i}}{\xi_{a_i}} (\tau_{s,a_i}^{n-1} - \tau_{s,a_i}^n) \right] + \Delta \Theta_{r,a_i}^n + \frac{m_{a_i}}{\xi_{a_i}} (\Delta \Theta_{r,a_i}^{n-1} - \Delta \Theta_{r,a_i}^n) / \Delta t, \quad (34)$$

$$r^{n+1,*} = r^n + \frac{\mathbf{D}}{k_B T} \left[f_s^n \Delta t + \frac{m \mathbf{D}}{k_B T} (f_s^{n-1} - f_s^n) \right] + R^n + \frac{m \mathbf{D}}{k_B T} (R^{n-1} - R^n) / \Delta t.$$

The calculation of the local coordinate systems, $\{a_i^{n+1,*}, b_i^{n+1,*}, c_i^{n+1,*}\}$, proceeds according to Eqs. (18) and (21)–(24). Using the coordinates, $r^{n+1,*}$ and $\{a_i^{n+1,*}, b_i^{n+1,*}, c_i^{n+1,*}\}$, we calculate estimates of the systematic forces, $f_s^{n+1,*}$, and torques, $\tau_{s,a_i}^{n+1,*}$, acting at the $(n+1)$ th time step. The final estimate of the rotations and position is made according to

$$\Delta \Theta_{a_i}^n = \frac{1}{2 \xi_{a_i}} \left[(\tau_{s,a_i}^n + \tau_{s,a_i}^{n+1,*}) \Delta t + \frac{m_{a_i}}{\xi_{a_i}} (\tau_{s,a_i}^{n-1} + \tau_{s,a_i}^{n,*} - \tau_{s,a_i}^n - \tau_{s,a_i}^{n+1,*}) \right] + \Delta \Theta_{r,a_i}^n + \frac{m_{a_i}}{\xi_{a_i}} (\Delta \Theta_{r,a_i}^{n-1} - \Delta \Theta_{r,a_i}^n) / \Delta t, \quad (35)$$

$$r^{n+1} = r^n + \frac{\mathbf{D}}{2 k_B T} \left[(f_s^{n+1,*} + f_s^n) \Delta t + \frac{m \mathbf{D}}{k_B T} (f_s^{n-1} + f_s^{n,*} - f_s^n - f_s^{n+1,*}) \right] + R^n + \frac{m \mathbf{D}}{k_B T} (R^{n-1} - R^n) / \Delta t.$$

Finally, the update of the local coordinate axes again proceeds according to Eqs. (18) and (21)–(24).

3. BD

The BD algorithm is implemented in a manner similar to the IBD algorithm:

$$\Delta\Theta_{a_i}^{n,*} = \frac{1}{\xi_{a_i}} \tau_{s,a_i}^n \Delta t + \Delta\Theta_{r,a_i}^n, \quad (36)$$

$$r^{n+1,*} = r^n + \frac{\mathbf{D}}{k_B T} f_s^n \Delta t + R^n,$$

where the R^n and the $\Delta\Theta_{r,a_i}^n$ are chosen as above for IBD. As before, the local coordinate axes, $\{a_i^{n+1,*}, b_i^{n+1,*}, c_i^{n+1,*}\}$, are updated according to Eqs. (18) and (21)–(24). The final update is given by

$$\Delta\Theta_{a_i}^n = \frac{1}{2\xi_{a_i}} (\tau_{s,a_i}^n + \tau_{s,a_i}^{n+1,*}) \Delta t + \Delta\Theta_{r,a_i}^n, \quad (37)$$

$$r^{n+1} = r^n + \frac{\mathbf{D}}{2k_B T} (f_s^n + f_s^{n+1,*}) \Delta t + R^n.$$

III. RESULTS

In the simulations discussed in the following below we study closed DNA loops with with the physiological superhelical density of $\sigma = -0.06$, represented using one hydrodynamic bead (or equivalently one DNA segment) per 12 bp. Our smallest system (600-bp, 50 segments, $L = 200$ nm) can adopt a superhelical form, but is also sufficiently small to make the generation of hundreds of trajectories on a workstation computationally feasible. For all the simulations considered here, the monovalent salt concentration is set at 0.04 M. All computations are performed on a 195 MHz/MIPS R10000 processor of a SGI Power Challenge computer. The eigenvalue decomposition was performed using the RS module from the EISPACK package.

To study the behavior of the model system in equilibrium, we generated several trajectories, each of length 1 ms, for each algorithm. In computing long trajectories, the hydrodynamic matrix (either the friction matrix or the diffusion matrix, depending on the algorithm) was not updated at every time step. Jian, Vologodskii, and Schlick¹⁰ find that it is possible to accurately reproduce equilibrium and dynamic properties while updating the diffusion matrix every 6 ns. We have reduced this value to 1 ns for all simulations reported here.

A. Computational performance

Table I reports the percentage of relative computational time that each algorithm devotes to calculations involving hydrodynamics (including the evaluation of the hydrodynamic matrix and its decomposition), interparticle forces, and all other steps in the update procedure. Because the hydrodynamic matrix is updated at a fixed simulation time interval, a greater proportion of CPU time is dedicated to the decomposition of this matrix as the time step is increased. Using $\Delta t = 100$ ps, we see that the LTID algorithm devotes about 39% of CPU time to performing the eigenmode decomposition. Another 50% of the CPU time is spent in the calculation of the matrices involved in the position and ve-

TABLE I. The distribution of CPU time for the three algorithms among hydrodynamic calculations (matrix evaluation and decomposition), interparticle force evaluation, and all other work (including matrix updates for LTID) as determined for a 50-bead (600-bp) system. The hydrodynamics calculations involve a Cholesky factorization for BD and IBD, and an eigen decomposition for LTID.

Method	Δt (ps)	% CPU, hydro	% CPU, force	% CPU, other
BD	10	7	17	75
	100	45	9	46
IBD	10	4	9	86
	100	27	7	66
LTID	10	23	4	73
	100	39	1	60

locity update Eqs. (28) and (29). For this case, only 1% of CPU time is dedicated to the calculation of interparticle forces. At the smaller time step, $\Delta t = 10$ ps, a greater proportion of CPU time (4%) is devoted to the calculation of forces, and the hydrodynamics calculations reduce to 23% of total CPU time.

The IBD algorithm at $\Delta t = 100$ ps dedicates 27% of its CPU time to the calculation and decomposition of the diffusion matrix, and nearly 70% of its CPU time to the matrix multiplications in the position update equation. Force calculations make up about 7% of total CPU time. BD involves a less complicated update step, with fewer matrix multiplications. Therefore BD spends a greater proportion of its CPU time (45%) on the Cholesky factorization of \mathbf{D} compared to IBD.

Table II reports the computational time involved in generating a 1 ms trajectory for the various algorithms. For each time step (10 and 100 ps), we see that BD requires the least computation and LTID the most. Note that for 10 ps time steps the CPU time associated with all methods is roughly of the same order of magnitude. However BD and IBD enjoy a speedup factor averaging 8 when the time step is increased to 100 ps, while the speedup for LTID is less than a factor of 2. This difference is due to the hydrodynamics update step, which is more costly for LTID than for either of the other algorithms. For a given trajectory length, hydrodynamic updates consume a fixed amount of CPU time, regardless of the time step.

TABLE II. Computational time for generating a 1 ms trajectory of the 50-bead (600-bp) system for a given algorithm and time step. Computational times are reported in hours on a 195 MHz/MIPS R10000 processor of a SGI Power Challenge computer. The speedup (last column) associated with increasing the time step from 10 to 100 ps is reported.

Method	Δt	CPU (h)	Speedup
BD	10	78	7
	100	10.9	
IBD	10	169	9
	100	19.2	
LTID	10	198	1.7
	100	114	

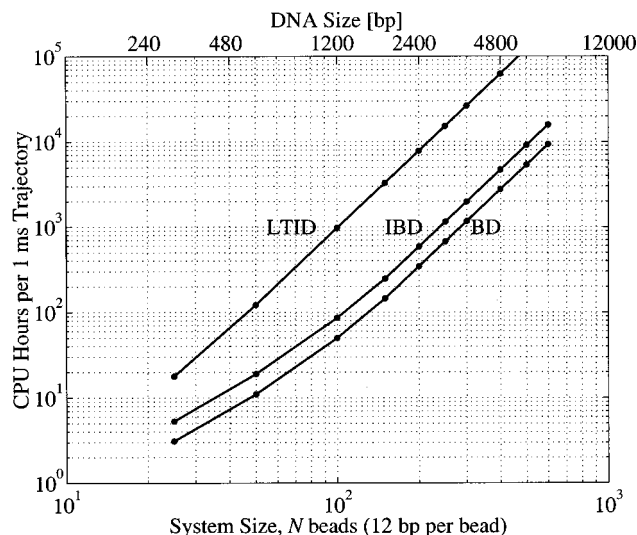


FIG. 1. Computational time associated with performing a 1 ms trajectory for the three methods as a function of system size, N , the number of beads. Computations are performed on a 195 MHz/MIPS R10000 processor of an SGI Power Challenge computer.

In Fig. 1 we plot the computational time associated with generating a 1 ms trajectory as a function of system size, N (number of beads), for each algorithm using $\Delta t = 100$ ps. For large N , LTID is more than an order of magnitude more expensive than either BD or IBD. As expected, CPU time grows as N^3 in the limit of large N . We also see that IBD is roughly twice as costly as BD.

B. Eigenvalue spectrum

The derivation of the IBD and BD algorithms depends on the assumption that both the numerical time step and the physical time scale of the system (e.g., for configurational evolution) are large compared to the time scale of the frictional decay of the inertial modes. To examine this assumption, we calculated the eigen decomposition of the friction matrix for a 600-bp system. This decomposition allows us to visualize the eigenmodes associated with an equilibrium structure.

For a 600-bp ($N = 50$) system, $\mathbf{M}^{-1}\mathbf{Z}$ is a 150×150 matrix, and has 150 independent eigenvalues, $\{\lambda_i\}$. The distribution of time constants, $\{\tau_i\} = \{\lambda_i^{-1}\}$, for a typical supercoil configuration is plotted in Fig. 2. Notice that most of the frictional modes (138 out of 150) have time constants less than 1 ps. In Fig. 3 we show the supercoil configuration and the eigenvectors associated with the eight largest time constants. The three largest relaxation times correspond to approximately rigid translational modes; the next three largest time constants correspond to motions that are mainly rotational. Unlike zero-frequency normal modes associated with a Hamiltonian system, the rigid-body modes of the friction tensor have finite eigenvalues, corresponding to the frictional decay times associated with these motions. More complex internal motions decay more rapidly and the associated time constants are all less than 1.5 ps. For the dynamics calculations presented in the following sections we use time steps of

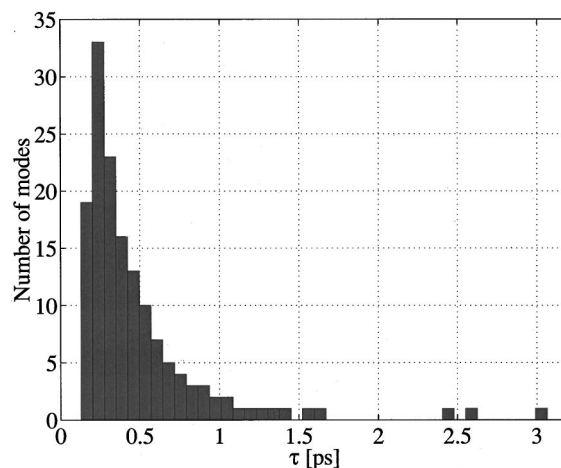


FIG. 2. The distribution of inertial relaxation times, $\{\tau_i\}$, for a typical configuration of a 600-bp minicircle model calculated as the inverse of the eigenvalues of the matrix $\mathbf{M}^{-1}\mathbf{Z}$. See also Fig. 3.

10 and 100 ps. For $\Delta t = 10$ ps, the product $\lambda_i \Delta t$ is greater than 3 for the rigid body modes and greater than 6 for the internal motion modes.

C. Slithering motion

Aside from being the basis of the LTID propagation scheme, the eigenmode decomposition allows us to explore

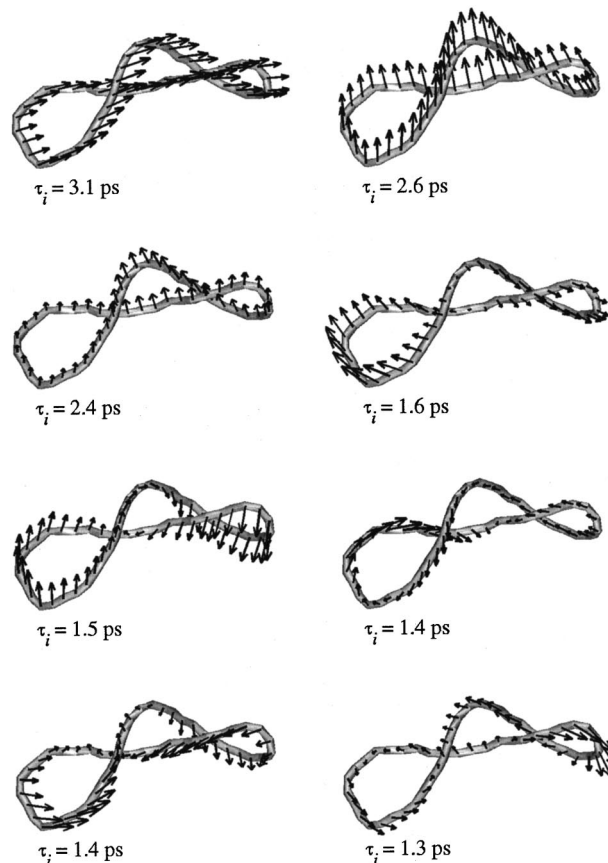


FIG. 3. Eigenmodes of a 600-bp (50-bead) supercoil. The eigenvectors associated with the eight largest inertial relaxation times (τ_i) are shown superimposed on top of the supercoil structure.

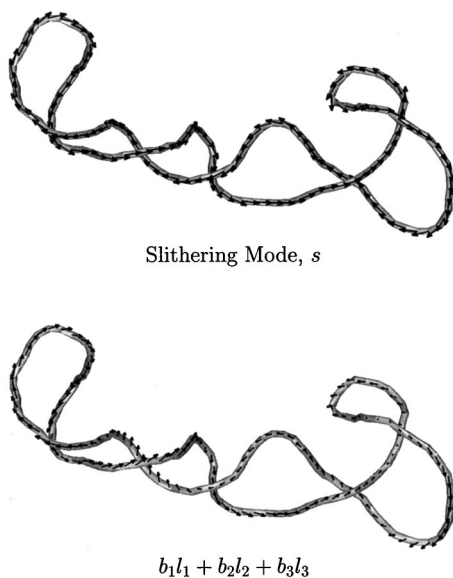


FIG. 4. Slithering of a 1500-bp supercoil. In the top panel, an equilibrium structure is shown, with the slithering mode, s , superimposed. The lower panel shows the motion described by summation of the three largest eigenmode contributions to s . See the text for details.

internal “slithering,” or a bidirectional conveyor-belt-like reptational motion in supercoiled DNA. We define slithering in our model as the concerted motion of the DNA beads in the direction of the helical axis. For the i th bead we calculate the slithering direction as $s_i = r_{i+1} - r_{i-1}$, and define $s \in Re^{3N}$ as the collective slithering mode for the N particles. This slithering mode is shown in the top panel of Fig. 4 for a DNA system of 1500 bp.

Denoting the eigenvectors contained in the matrix \mathbf{L} (see Sec. II C 1) as l_j , we decompose s using the linear combination

$$s = \sum_{j=1}^{3N} b_j l_j, \quad (38)$$

where the scalars $\{b_j\}$ are computed from the inner products

$$b_j = s l_j. \quad (39)$$

The coefficients $\{b_j\}$ are sorted according to descending absolute value, and their relative magnitudes are plotted in the top panel of Fig. 5, with the first ten values highlighted in the inset. The lower panel of Fig. 5 shows the time constants associated with the various eigenmodes. Again, the first ten values are highlighted in the inset. Slithering motion is not described by a single mode than can be independently excited, but it can be represented approximately by combining the first few k modes:

$$s_k = \sum_{j=1}^k b_j l_j.$$

For example, the motion described by s_3 is shown in the lower panel of Fig. 4. From Fig. 5 we see that these modes have approximately equal time constants of about 1.5 ps.

Therefore slithering motion decays with a time constant, τ_s , of about 1.5 ps. Using this value with the relation $D_s = k_B T \tau_s / Nm$ (where m is the bead mass) we can calculate

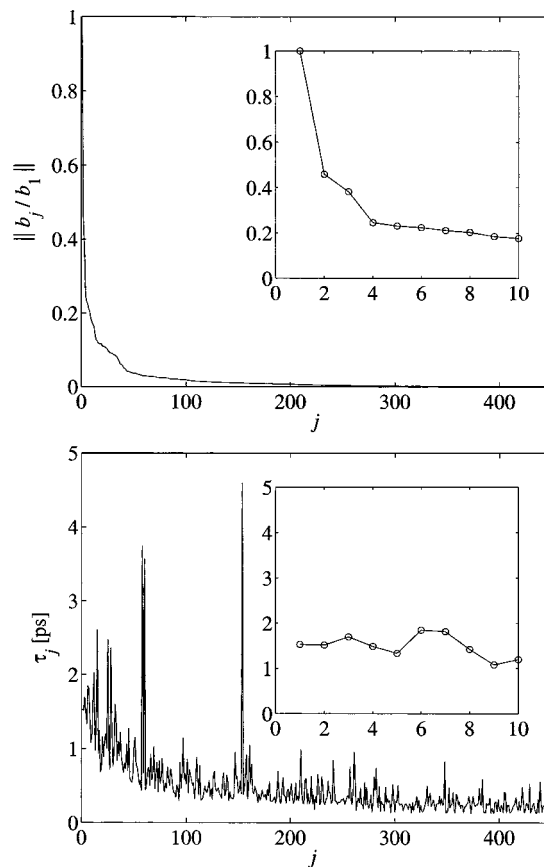


FIG. 5. Decomposition of the slithering mode for the 1500-bp DNA system. Upper panel: The relative magnitude of coefficients $\{b_j\}$ are plotted in descending order. Lower panel: The time constants $\{\tau_j\}$ for the eigenmodes associated with each $\{b_j\}$ are plotted. The insets show the magnitudes and the time constants for the first ten modes.

an effective slithering diffusion coefficient: $D_s \approx 2 \times 10^{-8} \text{ cm}^2/\text{s}$. From this estimate we can calculate the time required to slither a given distance. For example, slithering a distance of 500 nm (the length of the DNA contour for a system of 1500 bp) would require an average time of $(500 \text{ nm})^2 / 2D_s$, or about 60 ms. Since the time for reptation scales approximately as the cube of the size of the polymer,²¹ we expect a 10 kbp plasmid to have a reptational turnover time of about 17 s. For the same size plasmid, Marko²² estimates a reptation time of 7 s. This reptation time is characteristic of the time required for linearly distant sites along the DNA contour to be brought into close proximity by pure slithering motion. Realistic motions of plasmids—involving local slithering combined with the creation, deletion, and sliding of branches—results in mean juxtaposition times that scale approximately as the square of the size of the plasmid.²²

D. Translational diffusion coefficients

We calculated the translational diffusion coefficients, D_t , from the dynamics trajectories based on each of the three algorithms for several different sizes of DNA supercoils. Diffusion coefficients were estimated from the trajectories of the mean square displacements of the center of mass. The center of mass was calculated from

TABLE III. Translational diffusion coefficients obtained by BD, IBD, and LTID for supercoiled DNA of various sizes.

DNA size (bp)	D_t ($\times 10^{-8}$ cm ² /s)		
	BD	IBD	LTID
600	12.03 ± 0.11	11.97 ± 0.11	12.05 ± 0.11
900	9.15 ± 0.09	9.18 ± 0.09	9.09 ± 0.08
1200	7.76 ± 0.06	7.74 ± 0.07	7.72 ± 0.07

$$r_{\text{c.m.}}^n = \frac{1}{N} \sum_{i=1}^N r_i^n, \quad (40)$$

and D_t was estimated from

$$D_t = \frac{N_s \Delta t}{t_s} \sum_{j=1}^{t_s/N_s \Delta t} \left(\frac{\|r_{\text{c.m.}}^{N_s j} - r_{\text{c.m.}}^{N_s(j-1)}\|^2}{6N_s \Delta t} \right), \quad (41)$$

where t_s is the total trajectory length, and N_s is the number of time steps between calculations of mean square displacement. A simulation extending to $t_s = 1 \mu\text{s}$ was used, and N_s was set to 1000 steps. For each estimate, five trajectories were simulated to ensure convergence and improve statistics.

Table III reports D_t for DNA systems of 600, 900, and 1200 bp calculated based on BD, IBD, and LTID. For each algorithm a time step of 100 ps was used. The estimates based on the different algorithms closely agree.

E. Equilibrium distributions

Plotted in the upper panel of Fig. 6 are the probability distributions of W_r and R_g for the LTID algorithm based on two different time steps for several 1 ms trajectories of the 600-bp system. For each time step a total of ten runs of 1 ms each were used to deduce the distributions. The triangles represent the distributions calculated using a time step of 100 ps, while the circles represent the distributions calculated from a time step of 10 ps. The canonical distributions of these quantities calculated using Monte Carlo (MC) methods as outlined recently in Ref. 23 are also plotted for comparison. We see that the LTID algorithm, using either time step, generates probability distributions that agree well with the MC distributions.

The equilibrium distributions of W_r and R_g computed from the ten IBD trajectories of length 1 ms for both time steps (middle panel, Fig. 6) agree with the MC distributions for trajectories computed using $\Delta t = 100$. However, the R_g distributions computed using $\Delta t = 10$ ps do not match the expected equilibrium distribution predicted by MC. This is because the IBD approximation is valid for time steps that are large compared to the inertial relaxation times. A time step of $\Delta t = 100$ is large enough so that $e^{-\lambda_i \Delta t}$ is negligibly small for all inertial relaxation times, λ_i , and the IBD algorithm samples the same configuration space as LTID and MC. Clearly, the time step $\Delta t = 10$ ps is not sufficiently large compared to the inertial relaxation times for the DNA system.

Corresponding results for the BD algorithm (lower panels of Fig. 6) show that the equilibrium probability distributions are correctly predicted. Because the BD scheme repro-

duces the canonical ensemble in the small-time-step (differential) limit, proper sampling of the configuration space does not degrade at $\Delta t = 10$ ps, as for IBD.

F. Equilibrium fluctuations

We next report on the autocorrelation functions of the macroscopic properties W_r and R_g computed from equilibrium trajectories. For each algorithm—LTID, IBD, and BD—using both $\Delta t = 10$ and 100 ps, we calculated the autocorrelation functions based on ten trajectories of 1 ms each of a 600-bp supercoil. For a given property $A(t)$, the autocorrelation function $C_A(\tau)$ is given by

$$C_A(\tau) = \frac{\langle [A(t-\tau) - \langle A(t) \rangle] \cdot [A(t) - \langle A(t) \rangle] \rangle}{\langle [A(t) - \langle A(t) \rangle]^2 \rangle^{1/2}}, \quad (42)$$

where the brackets $\langle \cdot \rangle$ indicate averages over time.

The average autocorrelation functions from all methods are shown in Fig. 7. We see that the writhe correlation, $C_{W_r}(\tau)$, decays much more rapidly than the correlation of the radius of gyration, $C_{R_g}(\tau)$. The LTID autocorrelation curves (upper panel) at the two time steps are nearly identical, and a further reduction in Δt does not effect either function. The solid curves (LTID, $\Delta t = 10$ ps) for both functions thus represent the correlation structure of the inertial system. We use these as a reference for evaluation of the IBD and BD results.

The IBD autocorrelation functions (Fig. 7, middle panel), in contrast, are sensitive to Δt . At $\Delta t = 100$ ps, the IBD W_r and R_g correlations accurately reproduce the correlation predicted by LTID (solid lines). However, the $C_{R_g}(\tau)$ memory is greatly exaggerated at $\Delta t = 10$ ps. This behavior is expected since we have shown¹ that the configuration space is not properly sampled by IBD with $\Delta t = 10$ ps.

The BD results (lower panel of Fig. 7) deviate from the correlation structure predicted by LTID at both time steps and by IBD at $\Delta t = 100$ ps. Specifically, the BD autocorrelation functions at the two time steps are nearly identical and do not approach the inertial dynamics curves. The decay in R_g correlation is significantly slower for BD than for the LTID or IBD.

By fitting the tails of the correlation curves with exponentials we estimate the correlation time constants τ_{W_r} and τ_{R_g} , for W_r and R_g , respectively, for all algorithms for each value of Δt . The estimates are presented in Table IV. In the small-time-step limit ($\Delta t = 10$ ps), LTID predicts correlation time constants of $\tau_{W_r} = 0.81 \mu\text{s}$ and $\tau_{R_g} = 4.8 \mu\text{s}$, for W_r and R_g , respectively. The IBD algorithm reproduces these inertial correlation times at $\Delta t = 100$ ps but not at $\Delta t = 10$ ps, as expected. BD underestimates τ_{R_g} by 10%, regardless of the time step. Therefore, IBD can be applied using long time steps competitive with BD, and still accurately approximate the effects of inertia on kinetic processes.

G. Site juxtaposition

We next study fluctuations in the distance between two sites on the DNA chain separated by a fixed contour length L_s . Plotted in Fig. 8 is a trajectory of the distance, $d(t)$,

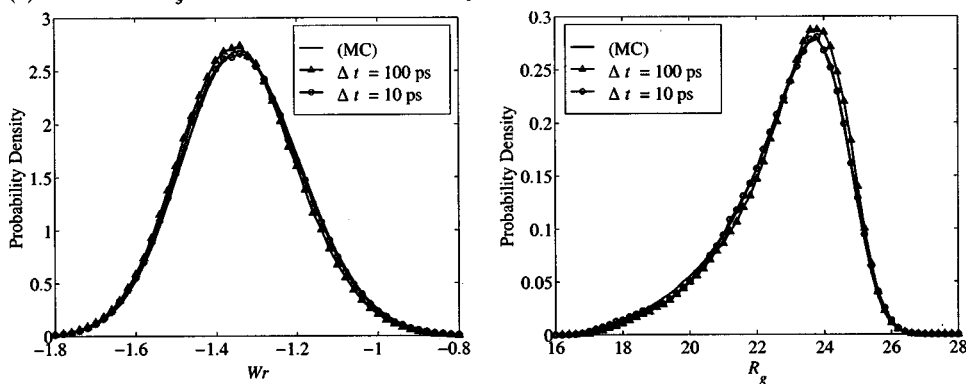
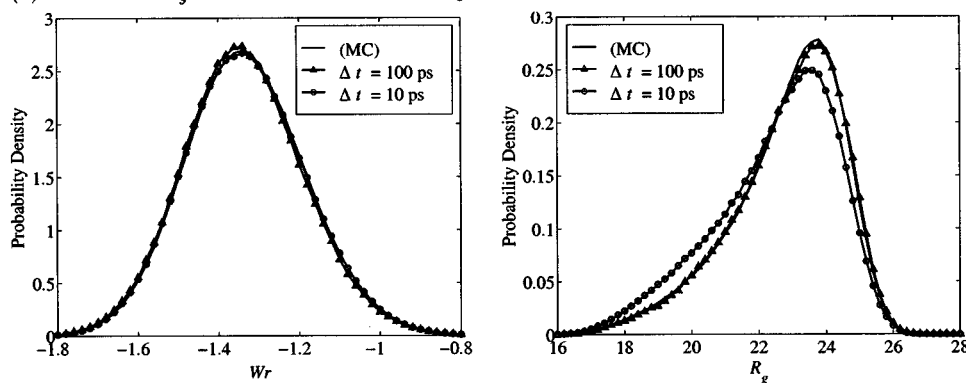
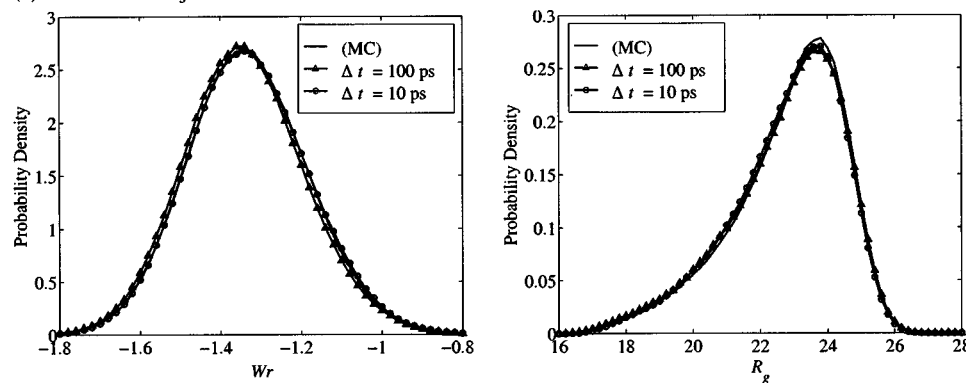
(a) Writhe and R_g distributions from LTID Trajectories:(b) Writhe and R_g distributions from IBD Trajectories:(c) Writhe and R_g distributions from BD Trajectories:

FIG. 6. Equilibrium distributions for LTID, IBD, and BD obtained from several trajectories of length 1 ms for W_r and R_g for the 600-bp DNA system. Ten trajectories were used for each time step.

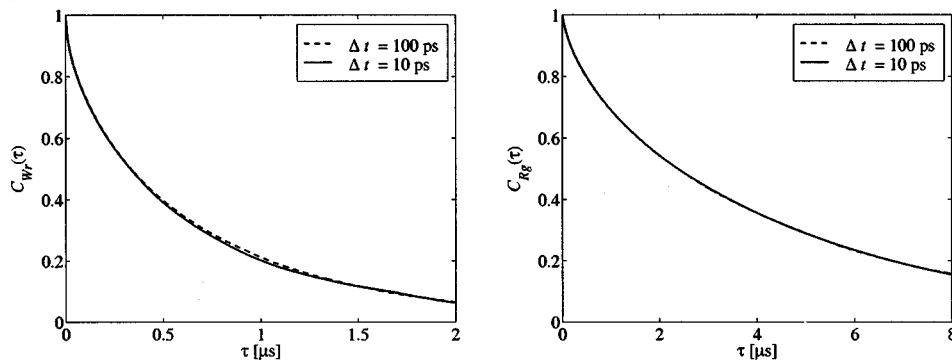
between two beads (beads number 10 and 35; $L_s = 300$ bp) in a 600-bp system from an IBD simulation using $\Delta t = 100$ ps. The distance between bead centers fluctuates between about 10 and 80 nm; the lower value corresponds to a typical definition of close approach, or ‘‘juxtaposition.’’⁸ The fluctuations tend to occur over a time scale on the order of tens to hundreds of microseconds. Also shown in Fig. 8 are the DNA configurations at four representative points along the trajectory, with the positions of beads 10 and 35 indicated by green spheres.

We define the juxtaposition time τ_j for two sites along the DNA contour as the time it takes for the distance between them to fall below a threshold d_0 . Thus, given some starting configuration, the juxtaposition time is the smallest positive value of t for which $d(t) \leq d_0$. To obtain the equilibrium mean $\langle \tau_j \rangle$, we computed several trajectories from

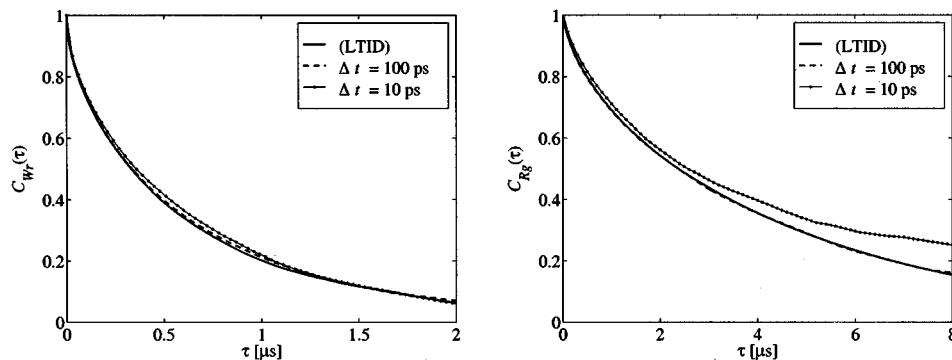
different equilibrium starting configurations until all pairs of beads separated by L_s bp had achieved juxtaposition.

For example, for a 1200-bp plasmid (modeled using 100 beads) we measured the time of first juxtaposition for all pairs of sites separated by the fixed contour length of $L_s = 300$ bp, or a contour separation of 25 beads. That is, given a starting configuration, we continued a trajectory until all 100 pairs of beads juxtaposed as defined by $d_0 = 10$ nm; each such juxtaposition gives a single measure of τ_j from one trajectory. To improve statistics, multiple trajectories were run, as follows. We ran 20 BD trajectories, yielding a total of 2000 measures of τ_j and an average juxtaposition time $\langle \tau_j \rangle = 0.343$ ms. Using the identical 20 starting configurations and 20 random seeds, we simulated the juxtaposition trajectories using IBD; an average juxtaposition time of 0.330 ms was obtained. A statistical analysis showed that the

(a) Autocorrelation functions from LTID Trajectories



(b) Autocorrelation functions from IBD Trajectories



(c) Autocorrelation functions from BD Trajectories

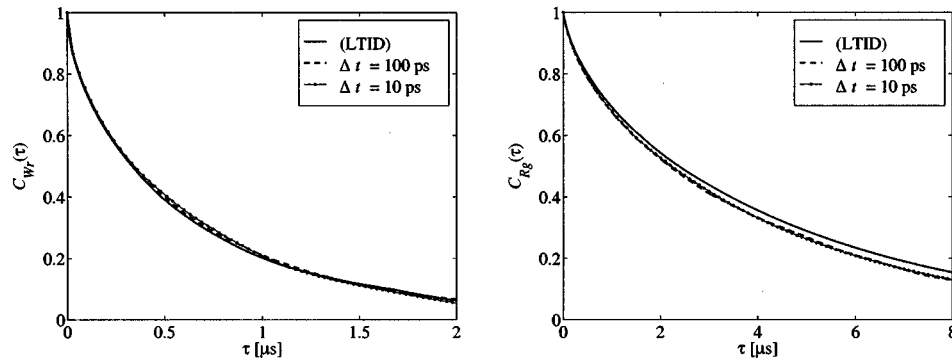


FIG. 7. Autocorrelation functions for LTID, IBD, and BD for W_r and R_g as calculated using time steps of 10 and 100 ps for a 600-bp system.

difference between these means is significant (Student's t -test, $p < 0.05$): juxtaposition occurs more rapidly, on average, in the inertial 1200-bp system than in the massless 1200-bp system.

Using a critical distance of $d_0 = 10$ nm, we also computed the mean juxtaposition times for contour lengths of 180, 240, and 300 bp along a 600-bp plasmid (Table V). The differences in estimated $\langle \tau_j \rangle$ between the two algorithms are not statistically significant for this much smaller system, and the dependence of $\langle \tau_j \rangle$ upon L_s is weak, as also deduced by Jian, Schlick, and Vologodskii.⁸ Table V also reports estimates of $\langle \tau_j \rangle$ for larger (900-, 1200-, and 1500-bp) plasmids with a site separation of 300 bp, and Fig. 9 displays $\langle \tau_j \rangle$ versus plasmid size (vertical bars indicate standard error). A statistically significant ($p < 0.05$) difference between the means is indicated by an asterisk.

Interestingly, for 1200- and 1500-bp plasmids the difference between BD and IBD predictions of $\langle \tau_j \rangle$ is non-negligible and significant. Intermolecular juxtaposition tends

to occur *more rapidly* in the inertial system than in the massless system. The difference in $\langle \tau_j \rangle$ between the inertial and noninertial case increases from 6% for a 1200-bp plasmid to 8% for a 1500-bp plasmid. For reference, also shown in the figure are juxtaposition times from Huang, Vologodskii, and

TABLE IV. Correlation time constants calculated for a 600-bp system by fitting the tails of the autocorrelation functions for W_r and R_g (Fig. 7) with exponentials.

Method	Δt (ps)	τ_{W_r} (μs)	τ_{R_g} (μs)
BD	10	0.77	4.3
	100	0.80	4.3
IBD	10	0.78	6.8
	100	0.81	4.8
LTID	10	0.81	4.8
	100	0.81	4.8

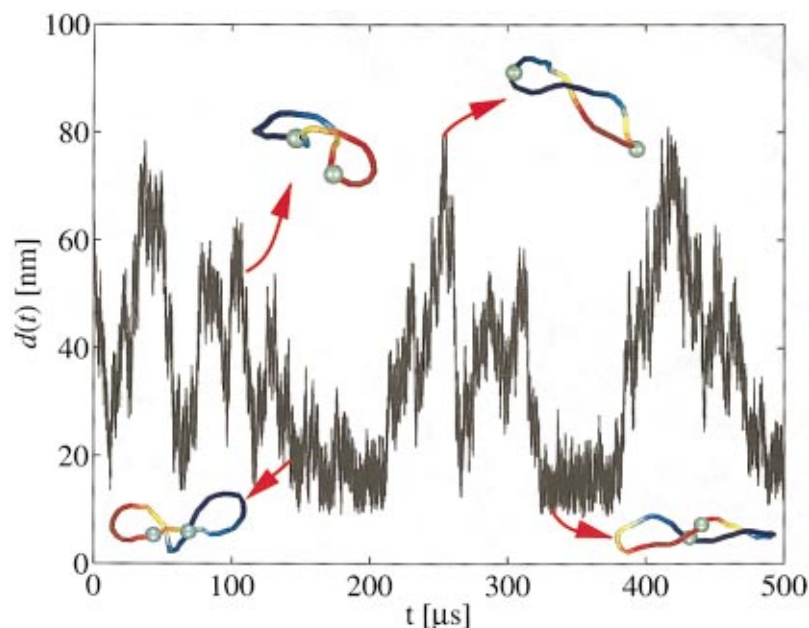


FIG. 8. (Color) The distance, d , between two selected sites separated by 300 bp in a 600-bp DNA minicircle is plotted vs time for an IBD trajectory using $\Delta t = 100$ ps. Also shown are the DNA configurations at four representative points in the trajectory, with the position of the selected sites indicated by green spheres.

Schlick (HVS)⁹ for the same system using BD with the same parameter values. Though the two BD programs are different, the agreement of the data of HVS data with our BD data is excellent. Also shown are data from Jian, Schlick, and Vologodskii,⁸ which were obtained using a different parameter set. Namely, we use the salt concentration of $C_s = 40$ mM and a torsional rigidity constant $C = 3 \times 10^{-12}$ erg nm, while they use $C_s = 10$ mM and $C = 2 \times 10^{-12}$ erg nm. As either C_s or C is increased, the DNA adopts a more interwound structure and juxtaposition times are reduced.

H. Folding dynamics

To determine whether the BD approximation influences kinetics of nonequilibrium processes in addition to equilibrium behavior, we examined the folding of DNA from a planar torsionally stressed circle into a relaxed supercoil. Previous studies have examined this relaxation process by Langevin dynamics²⁴ and Brownian dynamics,^{12,25} based on a limited number (less than 5) of trajectories. Here we computed ensembles of several hundred folding trajectories for

TABLE V. Mean juxtaposition times for various separation contour lengths L_s (see the text) along plasmids ranging in size from 600 to 1500 bp, as computed by BD and IBD. Where statistically significant, the relative difference between the mean times is reported in the rightmost column. See also Fig. 9.

DNA size (bp)	L_s (bp)	$\langle \tau_j \rangle$ (μ s) (BD)	$\langle \tau_j \rangle$ (μ s) (IBD)	(%)
600	180	88.2 ± 3.8	88.6 ± 3.9	–
	240	87.6 ± 3.8	88.1 ± 3.8	–
	300	93.0 ± 5.5	93.2 ± 5.6	–
900	300	237.6 ± 7.2	230.4 ± 6.9	–
1200	300	343.0 ± 7.7	324.9 ± 7.6	6
1500	300	430.5 ± 9.1	399.8 ± 8.8	8

LTID, IBD, and BD to elucidate statistical differences between the behavior predicted by these algorithms.

Snapshots from a typical folding trajectory (computed using LTID with $\Delta t = 10$ ps) are shown in Fig. 10 for a 600 bp DNA. The starting configuration is a planar circle with $Wr = 0$ and $R_g = 31.83$ nm (equal to the radius of the circle). This configuration is not present in the equilibrium ensemble because these values of Wr and R_g do not occur in the equilibrium distributions.¹ As the supercoil relaxes, values appropriate for the equilibrium ensemble are obtained within 4μ s.

This single trajectory only represents one possible folding pathway. The relaxation time scale must be evaluated from a statistical ensemble. We therefore calculated 500 such trajectories from LTID and IBD and 1000 from BD using the

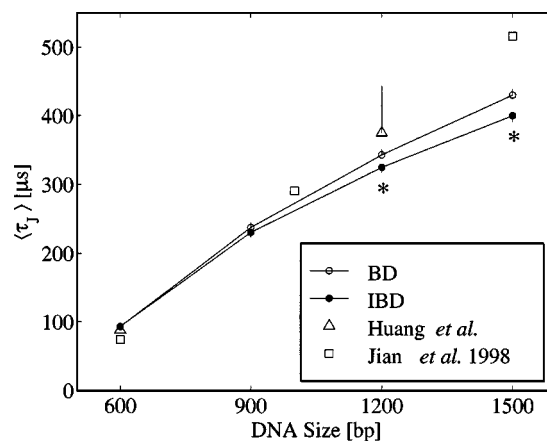


FIG. 9. Mean times of juxtaposition of two sites separated by 300 bp vs the length of the DNA plasmid (600–1500 bp) as computed by IBD and BD at $\Delta t = 100$ ps. Vertical bars indicate standard error. The critical distance of $d_0 = 10$ nm is used to determine juxtaposition, as outlined in the text. A statistically significant difference ($p < 0.05$ for t -test) between the means is indicated by an asterisk. BD data from Huang, Vologodskii, and Schlick (Ref. 9) and Jian, Schlick, and Vologodskii (Ref. 8) are shown for reference. See the text note on differences in models.

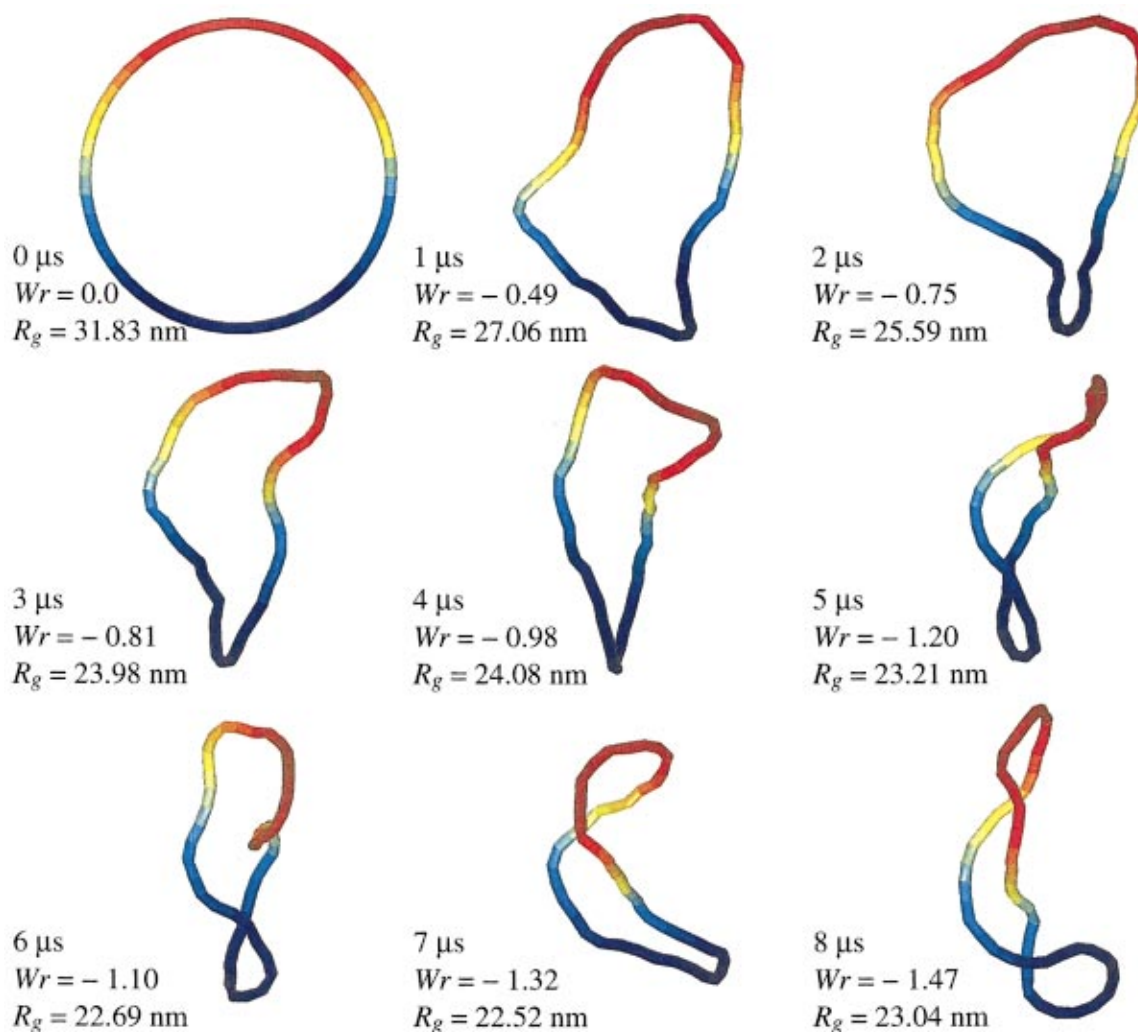


FIG. 10. (Color) Simulation snapshots of 600-bp supercoil relaxation as computed by LTID with $\Delta t = 10$ ps. The eight images, at $1 \mu\text{s}$ intervals, show relaxation from a planar circle to an equilibrium structure. The planar circle has $Wr = 0$, and $R_g = 31.83$ nm, which is equal to the radius of the circle.

same starting configuration, but different random seeds (for the random force). Figure 11 shows Wr (left) and R_g (right) as functions of time (black lines) for ten of these trajectories. For BD and IBD we used $\Delta t = 100$ ps and for LTID we used $\Delta t = 10$ ps.

The means over each total ensemble of trajectories are plotted Fig. 11 as solid red lines. The means plus and minus one standard deviation are plotted as dashed red lines; and the equilibrium means of Wr and R_g are indicated by horizontal black lines.

We find that the mean Wr of the LTID ensemble of trajectories relaxes to the equilibrium mean in about $6 \mu\text{s}$. This time scale is substantially longer than the time scale of equilibrium fluctuations in Wr (see Table I).

The radius of gyration, on the other hand, takes even longer to decay. Between 3 and $20 \mu\text{s}$, the mean curve undershoots the equilibrium mean, indicating an ensemble of structures that are, on average, more compact than in equilibrium. Only after $20 \mu\text{s}$ does the ensemble mean of R_g reach equilibrium. Again, the relaxation time is longer than the correlation times reported in Table I.

The mean curves for IBD (based on 500 trajectories)

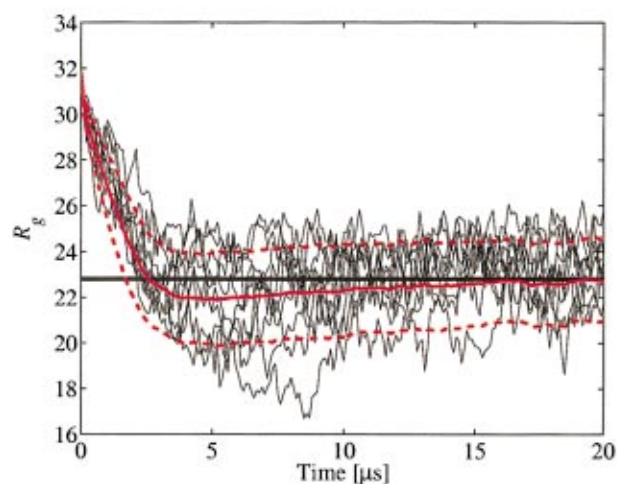
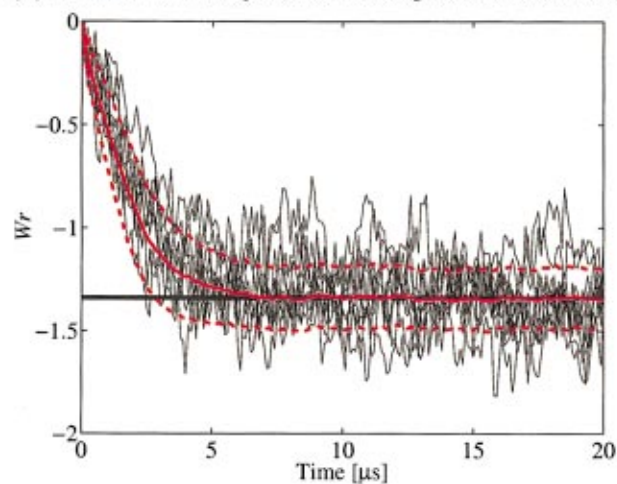
behave similarly to the mean relaxation curves obtained from LTID. Writhe relaxes to the equilibrium distribution in less than $10 \mu\text{s}$; while mean R_g undershoots the equilibrium mean for most of the $20 \mu\text{s}$. The BD writhe and R_g evolution and corresponding ensemble means are qualitatively similar to those generated by LTID and IBD.

Minor quantitative differences become apparent when the mean curves for all of the algorithms are plotted together in Fig. 12. Here, Wr and R_g are plotted as the ensemble mean trajectory minus the equilibrium mean. The ensembles from the different algorithms follow similar folding trajectories. The ensemble mean Wr relaxation curves are indistinguishable between the Brownian and Langevin descriptions, and only small differences are apparent in the R_g relaxations. Therefore, the differences between the LTID, IBD, and BD trajectories are not significant in the finite ensembles computed here.

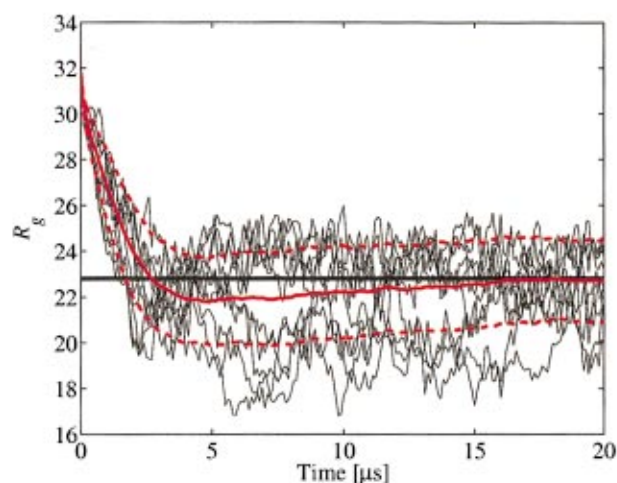
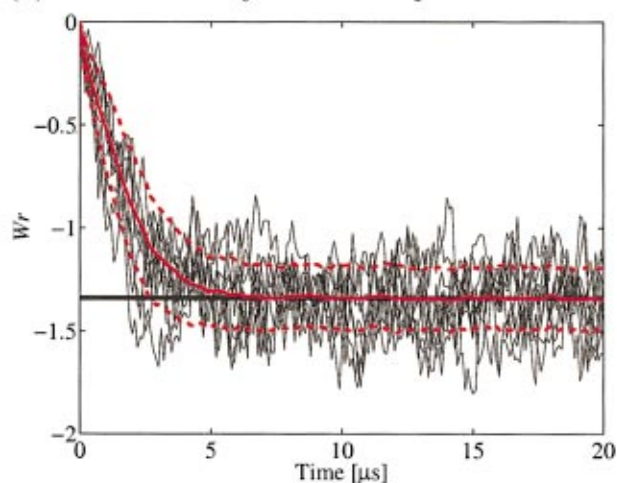
IV. DISCUSSION

We have shown that biologically important motions of supercoiled DNA plasmids as governed by Langevin dynam-

(a) Relaxation Trajectories Computed from LTID



(b) Relaxation Trajectories Computed from IBD



(c) Relaxation Trajectories Computed from BD

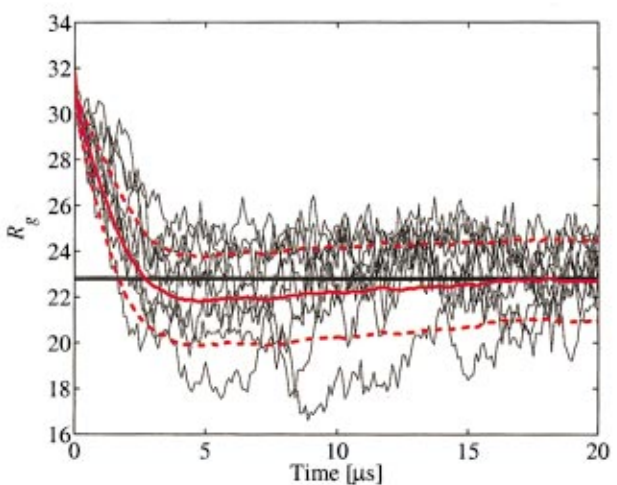
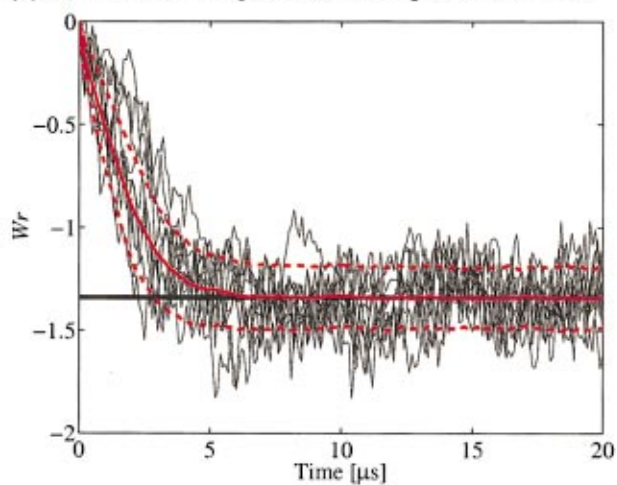


FIG. 11. (Color) Ensemble relaxation trajectories for W_r and R_g calculated using LTID (500 trajectories; $\Delta t = 10$ ps), IBD (500 trajectories; $\Delta t = 100$ ps), and BD (1000 trajectories; $\Delta t = 100$ ps) for a 600-bp plasmid. In each plot, the thin black curves denote data from the ten arbitrarily selected trajectories. Solid red lines indicate the ensemble mean over the entire collection of trajectories; dashed red lines indicate the mean plus/minus one standard deviation. Equilibrium means are indicated by horizontal black lines.

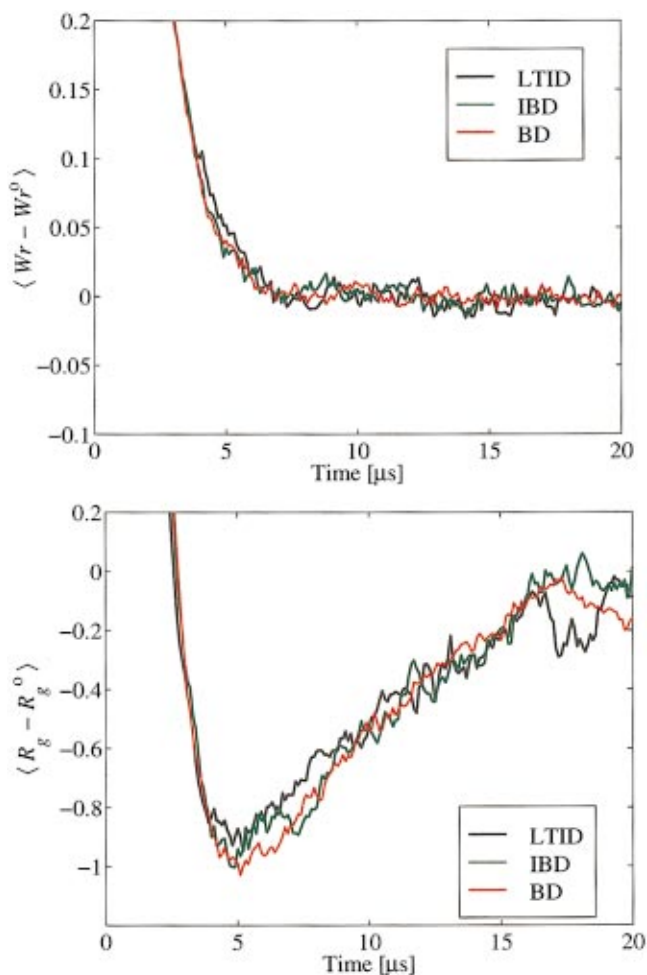


FIG. 12. (Color) Mean relaxations for Wr and R_g for LTID, IBD, and BD as computed by the same protocol described for Fig. 11 for the 600-bp system. The relaxation curves are nearly identical for the three algorithms.

ics depend on inertial effects which are ignored by the usual BD approach. A cursory inspection of this result may lead to an apparent contradiction. That is, if the polymer has inertial properties, should not the viscous solvent as well? If this were so, our use of the configuration-dependent friction tensor would be inappropriate since it is derived under the assumption of Stokes flow. However, it is well known that the motion of DNA systems take place at very low Reynolds numbers where the Stokes approximation is valid. However, that the fluid equations reduce to a noninertial form does not imply that the equation for polymer dynamics necessarily will. The amount of effective damping in the Langevin equation determines whether or not the Brownian approximation is accurate. As we discuss in the companion paper, the level of effective damping depends not only on the inertial relaxation times (which depend only on the masses of the particles and the friction tensor), but also on the potential energy function of the polymer, which is independent of the equations that govern the motions of the solvating fluid.

Our new algorithms, LTID and IBD, allow us to calculate long-time dynamic trajectories of elastic models of supercoiled DNA. These methods are similar to the BD algorithm of Ermak and McCammon² and variations thereof²⁶ in

that they allow relatively long time steps in computing the motions of a macromolecule governed by the Langevin equation with hydrodynamics. In LTID and IBD, as well as in the BD formulation, the motions of the particles are coupled through the potential energy function, which governs the interparticle forces, and also through the action of a configuration-dependent hydrodynamic interaction tensor. In contrast to BD, LTID and IBD have been developed without assuming that the dynamical system is fully damped, or noninertial.¹

The relative importance of inertia clearly depends upon the property under investigation. Figure 6 shows that LTID, IBD, BD, and MC all sample the same equilibrium distributions, providing convincing evidence that our new inertial algorithms produce valid results. While we expect the standard Brownian description to be poor when fluctuations in interparticle forces occur over a time scale that is similar to (or faster than) the momentum relaxation times, the effects of inertia on the behavior of our DNA model are not revealed when the equilibrium distributions predicted by the various algorithms are compared (Fig. 6). Nor are the ensemble average folding trajectories of the 600-bp plasmid strongly mass dependent (Fig. 12). Configurational transition rates in equilibrium, however, are sensitive to mass. For fluctuations around equilibrium conformations, differences in the writhing number and radius of gyration autocorrelation function are noted for the various algorithms (Fig. 7). Namely, the autocorrelation decay of R_g is faster for the noninertial (BD) case than for the inertial (LTID, IBD) cases, with τ_{R_g} about $0.5 \mu\text{s}$ (10%) smaller for BD trajectories than for LTID trajectories. Thus, high-frequency noise is overexaggerated in the BD case compared to IBD, leading to a faster decay of R_g memory.

Unfortunately, LTID cannot compete with BD in terms of efficiency. For $\Delta t = 100$ ps, LTID requires an order of magnitude more CPU time than BD to compute a trajectory of a fixed length for our 600-bp system (Table II). For larger systems, LTID requires about 15 times the computational time than BD (see Fig. 1). Investigations of the rate of site juxtaposition require the calculation of several trajectories of millisecond length,⁸ which are not feasible using LTID.

On the other hand, the IBD algorithm, derived based on a discretization of the Langevin equation or equivalently from a singular perturbation of the Langevin equation (see the companion paper¹), is much cheaper than LTID since IBD captures the inertial effects in a single mass-dependent term (proportional to the time derivative of the systematic force) in the position update equation. Thus IBD, an alternative to the standard BD scheme, can be used to study dynamics on time scales competitive with BD. The decision to treat dynamics as noninertial need not, therefore, be imposed by limitations on computational resources. Instead, the determination of whether to include mass can be made based on physical reasoning. Indeed, using IBD, we have been able to generate trajectories of relatively large systems (up to 1500 bp) over time scales of several milliseconds.

From these long trajectories we find that, for small (600 bp) DNA, neglecting inertia has little effect on the speed of the fluctuations in intermolecular distances (Table V); but in

larger systems the effects of mass are apparent in the juxtaposition times (Table V, Fig. 9). Simulating a 1200-bp plasmid using IBD results in mean juxtaposition times that are 6% smaller than the mean times predicted by BD. For 1500 bp, this difference increases to 8%. Clearly, inertial effects become more important as the system size is increased and momentum relaxation times increase, and thus the Brownian approximation becomes less accurate. Biological systems of interest can be 10 000 bp and longer.

As is the case for general Langevin integrators,²⁷ the IBD algorithm works with a time step that is neither too large nor too small. With the large time step $\Delta t = 100$ ps, the IBD algorithm appropriately samples the configuration space and reproduces the correlation structure of W_r and R_g when compared to the behavior of the inertial system. The IBD approximation is not accurate, however, in the small-time-step limit. Just as for the small-time-step behavior of the simple harmonic oscillator presented in the companion paper,¹ IBD fails to sample the canonical ensemble at $\Delta t = 10$ ps (Fig. 6). This behavior can be understood if we note that IBD is derived in the long-time-step limit of the LTID difference equations or as a long-time-step expansion of Langevin dynamics.

In conclusion, for small plasmids, inertia influences the thermal motions of DNA. The effects of inertia are most apparent on the rate of configurational transitions in equilibrium. While the kinetics of equilibrium fluctuations between global configurations (as measured by W_r and R_g fluctuations and by mean intermolecular juxtaposition times) are mass dependent, the mean pathway of relaxation from a perturbed state to equilibrium is not.

Interestingly, the Brownian approximation increases the rate of fluctuations in R_g (a process that occurs on the microsecond time scale) but decreases the rate of intermolecular site juxtaposition (millisecond time scale). As it is difficult to predict *a priori* the effects of inertia on a given process, IBD is recommended for computing trajectories of overdamped macromolecular systems governed by Langevin dynamics at time steps comparable with those used with BD. Important applications of IBD are calculations involving many trajectories of millisecond length in order to study the kinetics of slowly evolving properties, such as the biologically important intermolecular juxtaposition of linearly distant sites. As we have seen, both for the DNA system and for

the simple harmonic oscillator,¹ application of IBD requires the proper calibration of the time step. This can be accomplished by comparison of equilibrium distributions to those generated from some other method such as Monte Carlo and by comparison of dynamic properties to those generated based on LTID.

ACKNOWLEDGMENTS

Support by the National Science Foundation (ASC-9157582, ASC-9704681, BIR-9318159) and the National Institutes of Health (R01 GM55164-01A2) is gratefully acknowledged. T.S. is an investigator of the Howard Hughes Medical Institute.

- ¹D. A. Beard and T. Schlick, *J. Chem. Phys.* **112**, 7313 (2000), preceding paper.
- ²D. L. Ermak and J. A. McCammon, *J. Chem. Phys.* **69**, 1352 (1978).
- ³R. R. Sinden, *DNA Structure and Function* (Academic, San Diego, CA, 1994).
- ⁴K. R. Benjamin, A. P. Abola, R. Kanaar, and N. R. Cozzarelli, *J. Mol. Biol.* **256**, 50 (1996).
- ⁵A. V. Vologodskii and N. R. Cozzarelli, *Biophys. J.* **70**, 2548 (1996).
- ⁶S. A. Wasserman and N. R. Cozzarelli, *Science* **232**, 951 (1986).
- ⁷R. Kanaar and N. R. Cozzarelli, *Curr. Opin. Struct. Biol.* **2**, 369 (1992).
- ⁸H. Jian, T. Schlick, and A. Vologodskii, *J. Mol. Biol.* **284**, 287 (1998).
- ⁹J. Huang, A. Vologodskii, and T. Schlick (unpublished).
- ¹⁰H. Jian, A. Vologodskii, and T. Schlick, *J. Comput. Phys.* **136**, 168 (1997).
- ¹¹S. A. Allison, R. Austin, and M. Hogan, *J. Chem. Phys.* **90**, 3843 (1989).
- ¹²G. Chirico and J. Langowski, *Biopolymers* **34**, 415 (1994).
- ¹³A. V. Vologodskii and N. R. Cozzarelli, *Annu. Rev. Biophys. Biomol. Struct.* **23**, 609 (1994).
- ¹⁴A. V. Vologodskii and N. R. Cozzarelli, *Curr. Opin. Struct. Biol.* **4**, 372 (1994).
- ¹⁵P. J. Heath, J. B. Clendenning, B. S. Fujimoto, and J. M. Schurr, *J. Mol. Biol.* **260**, 718 (1996).
- ¹⁶P. J. Hagerman, *Annu. Rev. Biophys. Biomol. Struct.* **17**, 265 (1988).
- ¹⁷D. Stigter, *Biopolymers* **16**, 1435 (1977).
- ¹⁸C. R. Cantor and P. R. Schimmel, *Biophysical Chemistry. Part III. The Behavior of Biological Macromolecules* (Freeman, New York, 1980).
- ¹⁹J. Rotne and S. Prager, *J. Chem. Phys.* **50**, 4831 (1969).
- ²⁰M. P. Allen and D. J. Tildesley, *Computer Simulation of Liquids* (Oxford University Press, New York, 1987).
- ²¹P. G. de Gennes, *J. Chem. Phys.* **55**, 572 (1971).
- ²²J. F. Marko, *Physica A* **244**, 263 (1997).
- ²³H. Jian, Ph.D. thesis, New York University, 1997.
- ²⁴T. Schlick and W. K. Olson, *J. Mol. Biol.* **223**, 1089 (1992).
- ²⁵G. Chirico and J. Langowski, *Biophys. J.* **71**, 955 (1996).
- ²⁶A. Iniesta and J. G. de la Torre, *J. Chem. Phys.* **92**, 2015 (1990).
- ²⁷R. W. Pastor, B. R. Brooks, and A. Szabo, *Mol. Phys.* **65**, 1409 (1988).